Cost-efficient Core-shell TS-1/Silicalite-1 Supported Au Catalysts: Towards Enhanced Stability for Propene Epoxidation with H_2 and O_2

Zhaoning Song[a], Xiang Feng[a,*], Nan Sheng[a], Dong Lin[a], Yichuan Li[a], Yibin Liu[a], Xiaobo Chen[a], De Chen[c], Xinggui Zhou[b] and Chaohe Yang[a]

[a] *State Key Laboratory of Heavy Oil Processing, School of Chemical Engineering, China University of Petroleum, Qingdao 266580, China.*

[b] *State Key Laboratory of Chemical Engineering, East China University of Science and Technology, Shanghai 200237, China.*

[c] *Department of Chemical Engineering, Norwegian University of Science and Technology, Trondheim 7491, Norway.*

Abstract: Designing cost-effective TS-1 with enhanced catalytic stability in direct propene epoxidation with H_2 and O_2 is attracting tremendous research interests. In this work, a novel hydrophobic TS-1/S-1 lamellar support with Ti-rich shell and Si-rich cores is first synthesized using trace amount of TPAOH template. The effect of TPAOH concentration on physico-chemical properties of catalyst is then investigated. Compared with conventional Au/TS-1, optimum Au/TS-1/S-1 catalyst exhibits fantastic catalytic stability for over 100 h and good PO formation rate of 140 $g_{POh}{}^{-1}kg_{Cat}{}^{-1}$. Furthermore, the intrinsic reason for the enhanced stability is elucidated by TGA, XPS, ^{29}Si NMR and FT-IR. It is found that the coke weight for Au/TS-1/S-1 is only 0.99 wt%, much lower than 4.9 wt% for Au/TS-1 catalyst. The refractory aromatic coke is also not formed. On the one hand, this could be due to the unique core-shell structure and the presence of mesopores, which reduce the long diffusion path. On the other hand, it is because of enhanced hydrophobicity. This work sheds new light on the design and synthesis of highly effective and cost-efficient Au/Ti-containing catalysts.

Keywords: propene epoxidation, stability, diffusion path, core-shell TS-1/Silicalite-1

1. Introduction

Propylene oxide (PO), which is an important propene derivative, is widely used in the manufacture of polyurethane and polyester resins. Compared with traditional chlorohydrin and other organic hydroperoxide processes, direct propene epoxidation with H_2 and O_2 to produce PO is more environmentally benign, simple and cost-efficient [1]. Meanwhile, gold catalysts exhibit excellent catalytic activity in many catalytic reactions [2, 3]. Since Au/TiO_2 catalyst was reported to achieve high PO selectivity in direct propene epoxidation with H_2 and O_2 in 1998 [4], extensive efforts have been made to design the efficient Au/Ti-containing catalysts such as Au/TS-1, Au/Ti-MCM-41. Au/Ti-MCM-48, Au/Ti-SiO_2, Au/Ti-TUD and Au/Ti-HMS [5-10]. Among the above Au/Ti-containing catalysts, Au/TS-1 with good hydrophobicity and tetra-coordinated Ti exhibits superior activity and stability. However, it is still difficult to avoid the disadvantage of rapid deactivation for traditional Au/TS-1 catalyst [1]. Therefore, designing a highly efficient Au/TS-1 catalyst with prominently improved catalytic stability and good activity is of prime scientific and industrial importance.

In our previous work [11, 12], the deactivation of Au/TS-1 catalyst is mainly found to be the micropore blocking caused by carbonaceous deposits. The carbonaceous deposits are formed by the initial PO adsorption on the catalyst surface and subsequent ring-opening, oligomerization, rearrangement, cracking and coupling reactions. This makes Au clusters inside micropores inaccessible to reactants [7, 13-15]. Therefore, enhancing the mass transfer by decreasing the diffusion path length of products inside zeolite is a promising scenario to this problem [16]. Based on the deactivation

mechanism, several preparation methods have been proposed to improve the stability of Au/TS-1 catalyst, such as synthesizing uncalcined TS-1 with blocked pores (TS-1-B) [17, 18] and nanocrystalline mesoporous titanium silicalite-1 (MTS-1) [19]. The rapid deactivation problem could be dramatically improved by depositing Au on external surfaces, shortening reactant/product diffusion length and increasing hydrophobicity. However, the present catalysts still cannot meet the requirements of industry, and the stability, C_3H_6 conversion together with H_2 efficiency still need to be improved [8, 19]. Therefore, new strategies are still highly desired to achieve better catalytic performance.

Besides the catalytic performance, the expensive synthetic cost of the above mentioned Au/TS-1 catalysts also hinders the application of Au/TS-1 catalyst. In recent years, low-cost synthesis of TS-1 support is attracting more attention [20, 21]. Recently, we reported a cost-effective small-sized mesoporous TS-1 (STS-1) support [22], and the Au/STS-1 catalyst shows similar propene epoxidation performance to that of conventional Au/TS-1. Unfortunately, there is no improved stability for Au/STS-1 catalyst compared with Au/TS-1. Therefore, designing cost-effective Au/TS-1 catalyst with enhanced catalytic stability and good catalytic activity is also of prime industrial and scientific importance[23].

In this work, a mesoporous TS-1/S-1 support with Ti-rich shell and Si-rich cores is first synthesized using trace amount of TPAOH template. The Au/TS-1/S-1 catalysts shows amazing catalytic stability over 100 h in direct propene epoxidation with H_2 and O_2. Moreover, the relationship between the physicochemical structure of Au/TS-1/S-1

catalyst and catalytic performance (i.e., PO selectivity and catalytic stability) is further elucidated. The unique core-shell structure, presence of mesopores together with higher hydrophobicity result in reduced coke formation and absence of refractory aromatic coke, inhibiting the side reactions and deactivation caused by blocking of micropores. This work sheds new light on the design and synthesis of highly effective and cost-efficient TS-1 catalysts that with high stability and activity.

2. Experimental

2.1 Catalyst Preparation

The preparation of silicalite-1 (S-1) seed was carried out according to the procedure reported in the literature [24]. The TS-1/S-1 support was synthesized as follows: 5 g n-butylamine (NBA, 99.5 wt %) and 0.2 g tetrapropylammonium hydroxide (TPAOH, 25 wt %) was dissolved in deionized water under stirring. Afterward, 10 g colloidal silica was added to the above solution. Meanwhile, 0.4 g titanium(IV) tetrabutoxide (TBOT, 99 wt %) was dissolved in 15ml isopropanol (IPA, 99.5 wt %). The mixture was added to the hydrolyzed solution of colloidal silica dropwise under vigorous stirring. Subsequently, 1 g S-1 seed was added to the aforementioned solution. The resulting mixture was placed into a Teflon-lined stainless steel autoclave and crystallized at 443 K for 72 h. Finally, the product was washed and centrifuged with distilled water, dried at 353 K overnight and calcined at 823 K for 6 h. The molar composition of the gel was as follows: SiO_2: TiO_2: TPAOH: n-butylamine: H_2O= 1.0: 0.024: 0.005-0.02: 0.73: 30. The conventional TS-1 with the same Si/Ti ratio was synthesized using hydrothermal method developed by Khomane et al [25].

Au/TS-1/S-1 and conventional Au/TS-1 catalysts were prepared by the deposition-precipitation method [26]. Typically, 0.1 g hydrogen tetrachloroaurate (IV) trihydrate ($HAuCl_4 \cdot 4H_2O$, 99.99%) was mixed with 50 mL deionized water. 0.5 g TS-1 support was added to the above solution. The mixture was stirred for 1 h at room temperature, and the slurry was then adjusted to the pH of 7.0 by 1 M and 0.1 M aqueous solution of NaOH and stirred at room temperature for 9 hours. The resulting catalyst was then separated by centrifugation (5000 rpm for 10 min), washed three times with 100ml deionized water and dried at 298K overnight under vacuum.

2.2 Characterization

The X-ray diffraction patterns (XRD) of TS-1 catalysts were collected on a X'pert PRO MPD diffractometer instrument using Cu-Kα radiation. The N_2 adsorption-desorption isotherms were measured on a Micromeritics ASAP 2020 instrument. The fourier transform infrared spectroscopy (FT-IR) spectra of the catalysts were obtained on a Nicolet NEXUS 670 spectrometer with KBr as background. The ultraviolet-visible spectroscopy (UV-vis) spectra from 200 to 800 nm was determined on a PerkinElmer Lambda 35 spectrophotometer, and pure $BaSO_4$ was used as reference. Au loading and Ti content were determined by the inductive coupled plasma optical emission spectrometry (ICP-OES) on an Agilent 730 ICP-OES spectrometer. The surface Ti content was determined by the X-ray photoelectron spectroscopy (XPS) on a Perkin-Elmer PHI 5000C ESCA system. The high resolution transmission electron microscopy (HRTEM) images were taken on a JEOL JSM-2100F microscope, and the scanning electron microscopy (SEM) images were obtained on a Hitachi S-4800 field-emission

scanning electron microscope. The weights of carbonaceous deposits were analyzed by thermogravimetric analysis (TGA, PerkinElmer TGA Pyris 1). The ^{29}Si solid-state MAS NMR measurements of TS-1 samples were performed using a Unity/Inova (Varian, 600 MHz) spectrometer.

2.3 Gas-phase propene epoxidation with H_2 and O_2

The direct propene epoxidation reaction was taken in a quartz tubular reactor (i.d. 8 mm) employing a feed containing C_3H_6, H_2, O_2 and N_2 with the flow rate of 3.5/3.5/3.5/24.5 $mL \cdot min^{-1}$. The space velocity is 14000 $mLh^{-1}g_{cat}^{-1}$. Au/TS-1/S-1 and conventional Au/TS-1 catalysts (0.15 g) were evaluated under atmospheric pressure at 200°C. The reactants and products were analyzed using two on-line GC (Agilent 6890). Hydrocarbons, H_2, O_2, N_2, CO_2 and H_2O were analyzed by GC equipped with TCD. It should be noted that CO_2 can be well-analyzed in this work. Propylene oxide, ethanal, propanal, acetone, acrolein and other oxygenates were analyzed by the other GC equipped with FID. Blank evaluations indicated that no PO was generated in the blank reactor.

Propene conversion = mol of (C_3-oxygenates + 2/3ethanal + CO_2/3)/mol of propene in the feed.

PO selectivity = mol of PO/mol of (C_3-oxygenates + 2/3ethanal + CO_2/3).

H_2 efficiency = mol of PO/mol of H_2 converted.

3. Results and Discussion

3.1. Cost-effective synthesis of the novel TS-1/S-1 material

Novel TS-1/S-1 sample with unique Ti-rich shell and Si-rich cores is synthesized

using S-1 zeolite as seed. The required amount of TPAOH template is about 1/30 of traditional process. The physicochemical properties of TS-1/S-1 and conventional TS-1 are then compared.

Fig. 1a shows the powder X-ray diffraction (XRD) spectra of TS-1/S-1 and conventional TS-1 samples. It is clear that TS-1/S-1 and TS-1 all show the characteristic diffraction peaks at 7.8°, 8.8°, 23.1°, 23.9° and 24.3°, corresponding to the five characteristic peaks of typical MFI topological structure. The sharp single diffraction peaks at $2\theta = 24.3°$ for the two samples indicate their orthorhombic symmetry, which is one of the special features of TS-1. This suggests the presence of Ti in the framework [27]. Fig. 1b shows the N_2 adsorption-desorption isotherms and pore-size distribution of TS-1/S-1 and TS-1 samples. The rapid elevation of the curve at $P/P_0 < 0.02$ indicates the existence of micropores [28]. For TS-1/S-1 sample, the adsorption-desorption curves exhibit typical IUPAC type IV isotherms with a H1 hysteresis loop, which indicates the existence of mesoporous pores with concentrated pore diameter distribution. The capillary condensation occurs at P/P_0 ranging from 0.8 to 0.99 is observed, which is due to multilayer adsorption of nitrogen molecules inside inter-crystalline mesoporous. Both the N_2 adsorption-desorption isotherms and the pore-size distributions demonstrate that the TS-1/S-1 sample contains mesoporous with diameters of ca. 3.4 nm. These results illustrate the micro-mesoporous hierarchical structure of TS-1/S-1 support.

(Fig. 1 should be inserted here)

For propene epoxidation with H_2 and O_2, the Ti species are quite essential [29, 30].

The environment of Ti inside or outside the framework of TS-1 can be investigated by FT-IR and UV-vis characterizations. Fig. 2 (a) shows the FT-IR spectra of TS-1/S-1 and TS-1 samples. The two samples have six typical characteristic peaks in the finger print region at 450, 550, 800, 960, 1100 and 1230 cm^{-1}, which are in agreement with the typical FT-IR spectra of TS-1 reported in literature [31, 32]. The peak at 960 cm^{-1} is considered to be the presence of the Si-O-Ti structure inside the framework. This result suggests that the Ti species can be effectively introduced into the framework of TS-1/S-1 with adding the trace amount of TPAOH template.

FT-IR spectra could only be used to verify whether Ti species are introduced into the framework of TS-1. The detailed composition of Ti species should be further determined by UV-vis spectra, as shown in Fig. 2 (b). It is clear that there are dominate adsorption peaks at ca. 220 nm for TS-1/S-1 and conventional TS-1 samples, confirming the presence of isolated tetracoordinated Ti species in the MFI framework[33]. For TS-1/S-1 sample, small adsorption peaks show up at 260 nm, indicating the existence of octahedrally coordinated Ti complexes[34].

(Fig. 2 should be inserted here)

The Ti content of TS-1/S-1 was determined by the inductive coupled plasma optical emission spectrometry (ICP-OES) and the Ti content on the surface of TS-1/S-1 was determined by X-ray photoelectron spectroscopy (XPS). The XPS and ICP results show that the Si/Ti molar ratio of 64.7 on the surface of TS-1/S-1 is obviously lower than that of 105.2 of the holistic zeolite, demonstrating the presence of a non-uniform Si/Ti molar ratio in TS-1/S-1 sample.

This phenomenon is confirmed by TEM images of the TS-1/S-1 sample and S-1 seed, as shown in Fig. 3. The S-1 seed crystals are visible in the central part of TS-1/S-1 crystals. The average particle size of the wrapped S-1 crystals in TS-1/S-1 is ca. 30 nm, which is much smaller than S-1(ca. 100 nm), indicating that the S-1 seed crystals are incompletely dissolved in the crystallization process. This could be related to the dissolution-recrystallization process of S-1 seeds during crystallization in alkaline environment [32, 35, 36]. After adding the S-1 seeds into the initial gel, the seeds are outside-in dissolved and the crystals grow based on the surface of the S-1 seeds. The Si-rich core part of TS-1/S-1 is comes from the incompletely dissolved S-1 seed and the Ti-rich shell part is rooted in the recrystallization process. According to the ICP, XPS and TEM results, we propose a possible schematic diagram of crystallization process as shown in Fig. 4. Furthermore, the average crystal size of TS-1/S-1 is ca. 220*130*80 nm, which is smaller than the size of TS-1 (ca. 500 nm). It suggests that adding seeds has remarkable effect on reducing the crystal size which is because the seeds with MFI crystal structure can provide more crystal nuclei [37-39].

(Fig. 3 should be inserted here)

(Fig. 4 should be inserted here)

Moreover, the HRTEM image of TS-1/S-1 in Fig. 5 ensures the conformity of the crystal structure and the connectivity of the pores between the TS-1 shell and the S-1 cores, which can effectively promote the mass transfer of the reactants and products.

(Fig. 5 should be inserted here)

3.2 Effect of TPAOH concentration on properties of TS-1/S-1

The TPAOH concentration, as an essential parameter during synthesis, could greatly affect the physico-chemical properties of TS-1 [40]. Normally, this TPAOH/SiO_2 ratio is 0.15-0.3 for conventional TS-1 synthesis. In this work, the TPAOH/SiO_2 molar ratio is significantly reduced to 0.005. Since TPAOH constitutes the large percentage of TS-1 cost, the greatly reduced TPAOH/SiO_2 ratio indicates the lower cost and better industrial potential.

Fig. 6 shows the XRD patterns of TS-1/S-1 samples with different TPAOH/SiO_2 molar ratios (i.e., 0, 0.005, 0.01 and 0.02). All samples show the sharp peaks at 2θ = 7.8°, 8.8 °, 23.0 °, 23.9 ° and 24.4 ° corresponding to the five characteristic peaks of typical MFI topological structure. The single peaks at 2θ = 24.4◦ in TS-1-TPA-0.005/S-1, TS-1-TPA-0.01/S-1 and TS-1-TPA-0.02/S-1 samples indicate that all the three samples have an orthorhombic symmetry. As opposed to orthorhombic symmetry, the double peak at 2θ = 24.3◦ in TS-1-TPA-0/S-1 (i.e., template free) indicates that the TS-1-TPA-0/S-1 crystal has a monoclinic symmetry [27].

(Fig. 6 should be inserted here)

Fig. 7a shows the FT-IR spectra of TS-1/S-1 samples with different TPAOH concentrations. The TS-1-TPA-0.005/S-1, TS-1-TPA-0.01/S-1 and TS-1-TPA-0.02/S-1 samples possess six typical characteristic peaks in the finger print region at 450, 550, 800, 960, 1100 and 1230 cm^{-1}, which are consistent with the typical FT-IR spectra of TS-1 reported in the literatures [31]. However, the absorption peak at 960 cm^{-1} which considered to be the presence of the Si-O-Ti structure inside the framework does not show up in the TS-1-TPA-0/S-1 sample. This is also confirmed by the UV-vis spectra

in Fig. 7b. It is clear that there are dominate adsorption peak at ca. 220 nm for TS-1-TPA-0.005/S-1, TS-1-TPA-0.01/S-1 and TS-1-TPA-0.02/S-1 samples, confirming the presence of isolated tetracoordinated Ti species in the MFI framework. Meanwhile, adsorption peaks also show up at 260 nm and edge down with the rise of TPAOH concentration, indicating that the octahedrally coordinated Ti complexes gradually decreased with the increase of TPAOH concentration. However, the weaker intensity of 220 nm adsorption peak and the stronger absorption peaks arise in 260 and 330 nm of TS-1-TPA-0/S-1, confirming that isolated tetracoordinated Ti is difficult to be introduced into the framework of TS-1-TPA-0/S-1 which is synthesized without adding TPAOH template. The possible reason should be the absence of TPA^+ in the synthesis system because TPA^+ has an important impact on the crystallization process as structure-directing effect.

(Fig. 7 should be inserted here)

Fig. 8 shows the TEM images of TS-1/S-1 samples with different TPAOH/SiO_2 molar ratios. The shape of the TS-1-TPA-0/S-1 is cuboid, while other TS-1/S-1 samples are six-sided lamellar with several cores inside. When TS-1/S-1 is synthesized without adding TPAOH template, the average crystal size is ca. 100 nm as shown in Fig. 7a. With the increase of the TPAOH concentration, the average crystal size increases from 220*130*80 nm to 330*180*110 nm. This could be because the addition of template agent is helpful for crystal growth.

(Fig. 8 should be inserted here)

Conventional TS-1 and TS-1/S-1 samples with different TPAOH/SiO_2 molar ratios

are used as supports for Au deposition. To make a fair comparison, the Au loadings of the catalysts are similar (ca. 0.10 wt%). Fig. 9 shows the HRTEM images of the Au/TS-1/S-1 with different TPAOH/SiO_2 molar ratios and Au/TS-1 catalysts. More than 150 nanoparticles were measured to determine Au average particle size to increase accuracy. It is found that the Au/TS-1 and Au/TS-1/S-1 catalysts show similar Au particle size of ca. 3.0 nm. This could exclude the effect of Au particle size [1, 4, 41, 42] and give an intrinsic effect of support.

(Fig. 9 should be inserted here)

The catalytic performance of the Au/TS-1/S-1 and the conventional Au/TS-1 catalysts for propene epoxidation are compared in Fig. 10a. The Au/TS-1 catalyst shows higher initial PO formation rate of 155 $g_{PO}h^{-1}kg_{Cat}^{-1}$. However, the PO formation rate sharply decreased from 155 to 106 $g_{PO}h^{-1}kg_{Cat}^{-1}$ in 20 h because the Au clusters inside the microporous channels are no longer accessible to reactants due to micropore blocking deactivation by carbonaceous deposits. In contrast, the Au/TS-1/S-1 catalysts show greatly improved stability over 100 h. The PO formation rate increased from 125 to 140 $g_{PO}h^{-1}kg_{Cat}^{-1}$ when TPAOH/SiO_2 molar ratio increases from 0.005 to 0.02. This could because TPA^+ is contribute to facilitate the tetracoordinated Ti into the framework of TS-1/S-1 [22], thus providing more Ti^{4+}active centers for the reaction.

The detailed products selectivities and H_2 efficiencies of the Au/TS-1/S-1 and the conventional Au/TS-1 catalysts are shown in Fig. 10b. With the increase of the TPAOH/SiO_2 molar ratio, the PO selectivity of Au/TS-1/S-1 catalyst grows slowly from 84.5% to 87.2%, which is slightly lower than that of the traditional Au/TS-1 catalyst

(ca. 89%). The main side product of Au/TS-1/S-1 catalyst is carbon dioxide. To verify whether the result is caused by S-1 cores, we investigated the effect of Au/S-1 catalyst on the catalytic performance. Compared with Au/TS-1/S-1, the Au/S-1 catalyst shows few PO formation rate of only 2.3 $g_{PO}h^{-1}kgCat^{-1}$ and negligible side products. This result indicates that the S-1 cores have little effect on the catalytic activity and selectivity. The slight decrease of the PO selectivity is most likely caused by the non-selective oxidation of propene and the deep oxidation of PO provided by non-framework [$HOTiO_3$] units [43-45]. It is noted that the reduction of selectivity is only less than 2%, and the selectivity can be increased by eliminating the non-framework Ti by acid treating [46].

In addition, with the increase of the TPAOH/SiO_2 molar ratio, the H_2 efficiency of Au/TS-1/S-1 catalyst increases from 19.8% to 21.9% and the C_3H_6 conversion increases from 4.05% to 4.51%. The H_2 efficiency and the C_3H_6 conversion of Au/TS-1/S-1 catalyst are still comparable to the conventional Au/TS-1 catalyst although small amount of octahedrally coordinated Ti species show up. It is reported that the decomposition of H_2O_2 is a predominant route to reduce the H_2 efficiency and the C_3H_6 conversion at high temperature of 200 °C [5, 47, 48]. Therefore, the shortened diffusion path of Au/TS-1/S-1 catalyst is beneficial to the transfer of H_2O_2 from Au to the adjacent Ti^{4+} sites, which hinders the decomposition of H_2O_2 caused by octahedrally coordinated Ti.

(Fig. 10 should be inserted here)

3.3 Intrinsic reasons for the unique stability of Au/TS-1/S-1 catalyst

In order to illustrate the intrinsic reasons for the superior catalytic stability of the

Au/TS-1/S-1 catalyst, the properties of the catalysts after reaction are further characterized. The TGA analysis of the Au/TS-1 and Au/TS-1-TPA-0.02/S-1 catalysts at 200 ºC after 20 h are shown in Fig. 11a. The total coke weight of the Au/TS-1/S-1 catalyst (0.99 wt %) is much lower than that of the Au/TS-1 catalyst (4.9 wt %), indicating that the Au/TS-1/S-1 catalyst is beneficial to inhibit the production of coke. It is reported that Au nanoparticles are mainly responsible for the formation of H_2O_2, and Ti^{4+} sites are responsible for propene epoxidation to PO by Ti-OOH intermediate [49]. Meanwhile, researchers generally agree that shortening the diffusion length in the catalyst can effectively reduce coke production [19]. Since the Ti^{4+} centers of the Au/TS-1/S-1 is concentrated on the shell of the support, Au nanoparticles are therefore mainly loaded on the shell of TS-1/S-1 support due to the synthesis mechanism of deposition-precipitation method [11]. Therefore, the products formed on TS-1 shell can more easily diffuse out to the gas phase. Moreover, when part of products inside TS-1 penetrate S-1 cores, the ring-opening reactions are inhibited possibly because silicalite-1 has low ability to catalyze ring-opening reactions [50]. Furthermore, the presence of mesopores may make more space for coke and hinder the micropore blocking. The DTG curves of the Au/TS-1 and Au/TS-1/S-1 catalysts are shown in Fig. 11b. The DTG peaks means the occurrence of different kinds of carbonaceous deposits on the catalyst. Generally, heavier carbonaceous deposits show up at higher temperature. The DTG peaks at 340 and 460°C show up for both catalysts. However, one of the DTG peaks for Au/TS-1 catalyst appears at 650 °C, indicating the existence of the refractory carbonaceous deposits. The absence of the peak at 650 °C for Au/TS-1/S-1 catalyst

indicates that the carbonaceous deposits on Au/TS-1/S-1 are much lighter than those on Au/TS-1 catalyst.

(Fig. 11 should be inserted here)

FT-IR is another technique to investigate the properties of carbonaceous deposits. Fig. 12 shows the FT-IR spectra of Au/TS-1 and Au/TS-1/S-1 catalysts at 200 ºC after 20 h. For the conventional Au/TS-1 catalyst, three absorption peaks are observed at 1350-1470, 1600-1650 and 1700-1750 cm^{-1}, which are resulted from the branched alkanes, polyalkenes and refractory aromatic species [51, 52], respectively. However, the absorption peak at 1700-1750 cm^{-1} (i.e., refractory aromatic species) is not observed from Au/TS-1/S-1 catalyst. This is in accordance with the above TGA results.

(Fig. 12 should be inserted here)

Moreover, we added a comparative experiment of Au/TS-1/SiO_2 to clarify the importance of the crystal structure conformity between the TS-1 shell and the S-1 cores. The TS-1/SiO_2 sample was synthesized with 30 nm solid SiO_2 sphere as the core. The synthetic method is similar to the literature developed by Zhang et al. [53] and Au/TS-1/SiO_2 catalyst was prepared by the deposition-precipitation method in the same way as in section 2.1. However, the Au/TS-1/SiO_2 catalyst shows initial PO formation rate of 94 $g_{PO}h^{-1}kg_{Cat}^{-1}$ and PO selectivity of only 47% in direct propene epoxidation with H_2 and O_2. Meanwhile, the Au/TS-1/SiO_2 catalyst deactivates rapidly from 94 $g_{PO}h^{-1}kg_{Cat}^{-1}$ to 55 $g_{PO}h^{-1}kg_{Cat}^{-1}$ in two hours. We suggest that the inconsistent crystal structure and the unconnected pores between the TS-1 shell and the SiO_2 core may be responsible for the low catalytic selectivity and stability. When part of the products

cannot diffuse through the SiO_2 core, the ring-opening reactions that lead to the formation of side products and coke may occur. This result verified the importance of the consistent crystal structure and the unconnected pores between shell and core. However, other factors may also affect the catalytic performance of Au/TS-1/SiO_2 catalyst, which deserves further discussion.

In addition to the mass transfer ability, hydrophobicity is also an important parameter affecting the properties of carbonaceous deposits. The ^{29}Si MAS NMR spectrum of TS-1 and TS-1/S-1 supports are shown in Fig. 13. The two spectrum all show the absence of $(SiO)_2Si(OH)_2(Q_2)$ resonances at ca. -80 to -90 ppm, indicating that there is no amorphization of the support framework. The signals at -113 and -116 ppm, which are attributed to typical $Si(OSi)_4(Q_4)$ species and the orthorhombic symmetry of zeolite, respectively, are observed in both catalysts [54]. The signal at -104 ppm in the spectrum of TS-1 corresponding to the $(SiO)_3SiOH(Q_3)$ species functionalized by hydroxyl groups is stronger than that of TS-1/S-1 [18, 55]. Based on the deconvolution and integration of the spectra, the percentages of peaks at -104 ppm are 5.8% for TS-1 and 1.1% for TS-1/S-1, suggesting that the TS-1/S-1 support has less hydroxyl groups than TS-1 support. This could be possibly because recrystallization can effectively convert Si-OH into Si-O-Ti. Less surface hydroxyl groups indicates better hydrophobicity, which is beneficial for the desorption of PO and suppression of side reactions on catalyst surface [19]. Besides better mass transfer ability, this higher hydrophobicity also gives explanation on the lower coke weight and absence of refractory aromatic coke of Au/TS-1/S-1 catalyst.

(Fig. 13 should be inserted here)

The catalytic performances of Au/TS-1/S-1 and other Au/Ti-containing catalysts in literature for propene epoxidation with H_2 and O_2 are compared in Table 1. It is clear that all the TS-1-based catalysts have good performance. However, TS-1/S-1 support with TS-1 shell and S-1 cores supported Au catalyst shows striking catalytic stability. From the above results, it can be seen that the hydrophobic core-shell structure and the mesopores of TS-1/S-1 support can provide enhanced mass transfer ability (shorter diffusion length, better PO desorption, coke accommodation space), which inhibits the coke formation and also deactivation caused by micropore blocking.

(Table 1 should be inserted here)

4. Conclusion

In summary, the cost-efficient TS-1/S-1 support with Ti-rich shell and Si-rich cores is successfully synthesized using trace amount of TPAOH template. It is found that the TPAOH/SiO_2 molar ratio can be reduced to only 0.005. Compared with conventional Au/TS-1 catalyst, the Au/TS-1/S-1 catalyst exhibits excellent catalytic stability over 100 h and good PO formation rate of 140 $g_{POh}^{-1}kg_{Cat}^{-1}$. The total coke weight of the Au/TS-1/S-1 catalyst (0.99 wt %) is much lower than that of the Au/TS-1 catalyst (4.9 wt %), indicating that the Au/ TS-1/S-1 catalyst is beneficial to inhibit the production of coke. The mechanism for the enhanced stability is due to the unique hydrophobic core-shell structure which shows enhanced mass transfer ability (i.e., shorter diffusion length, higher hydrophobicity, presence of mesopores). In this way, the coke is less and

deactivation caused by blocking of micropore is inhibited. This work is of significant importance on the design and synthesis of highly stable and cost-efficient TS-1 catalysts.

Acknowledgments

This work is financially supported by the Natural Science Foundation of China (21606254); Natural Science Foundation of Shandong Province (ZR2016BB16); Key research and development plan of Shandong Province (2017GSF17126); Fundamental Research Funds for the Central Universities (18CX02014A, 18CX02130A); Independent innovation foundation of Qingdao (17-1-1-18-jch); Applied basic research programs of Qingdao city (16-5-1-28-jch) and support by Chambroad Chemical Industry Research Institute CO., LTD.

References

1. W.S. Lee, M.C. Akatay, E.A. Stach, F.H. Ribeiro, W.N. Delgass, Reproducible preparation of Au/TS-1 with high reaction rate for gas phase epoxidation of propylene, J. Catal. 287 (2012) 178-189.

2. F.Z. Su, Y.M. Liu, L.C. Wang, Y. Cao, H.Y. He, Ga-Al mixed-oxide-supported gold nanoparticles with enhanced activity for aerobic alcohol oxidation, Angew. Chem. Int. Edit. 120 (2008) 340-343.

3. X. Liu, L. He, Y.M. Liu, Y. Cao, Supported gold catalysis: from small molecule activation to green chemical synthesis, Accounts. Chem. Res. 47 (2013) 793-804.

4. M. Haruta, B.S. Uphade, S. Tsubota, A. Miyamoto, Selective oxidation of propylene over gold deposited on titanium-based oxides, Res. Chem. Intermed. 24 (1998) 329-336

5. W.S. Lee, L.C. Lai, M.C. Akatay, E.A. Stach, F.H. Ribeiro, W.N. Delgass, Probing the gold active sites in Au/TS-1 for gas-phase epoxidation of propylene in the presence of hydrogen and oxygen, J. Catal. 296 (2012) 31-42.

6. B.S. Uphade, Y. Yamada, T. Akita, T. Nakamura, M. Haruta, Synthesis and characterization of Ti-MCM-41 and vapor-phase epoxidation of propylene using H_2 and O_2 over Au/Ti-MCM-41, Appl. Catal. A-Gen. 215 (2001) 137-148.

7. B.S. Uphade, T. Akita, T. Nakamura, M. Haruta, Vapor-phase epoxidation of propene using H_2 and O_2 over Au/Ti-MCM-48, J. Catal. 209 (2002) 331–340.

8. J. Chen, S.J. Halin, E.A. Pidko, M. Verhoeven, D.M.P. Ferrandez, E.J. Hensen, J.C. Schouten, T.A. Nijhuis, Enhancement of catalyst performance in the direct propene epoxidation: a study into gold–titanium synergy, ChemCatChem 5 (2013) 467-478.

9. J. Lu, X. Zhang, J.J. Bravo-Suárez, K.K. Bando, T. Fujitani, S.T. Oyama, Direct propylene epoxidation over barium-promoted Au/Ti-TUD catalysts with H_2 and O_2: effect of Au particle size, J. Catal. 250 (2007) 350–359

10. H. Song, G. Li, X. Wang, Y. Chen, Characterization and catalytic performance of Au/Ti-HMS for direct generation of H_2O_2 and in situ-H_2O_2-ODS from H_2 and O_2: an in situ-reduction synthesis and a recycle study of catalyst, Micropor. Mesopor. Mat. 139 (2011) 104-109.

11. X. Feng, X. Duan, G. Qian, X. Zhou, D. Chen, W. Yuan, Au nanoparticles deposited on the external surfaces of TS-1: enhanced stability and activity for direct propylene epoxidation with H_2 and O_2, Appl. Catal. B 150–151 (2014) 396–401.

12. Z. Song, X. Feng, Y. Liu, C. Yang, X. Zhou, Advances in manipulation of catalyst structure and relationship of structure-performance for direct propene epoxidation with H_2 and O_2, Prog. Chem. 28 (2016) 1762-1773.

13. J. Huang, T. Takei, T. Akita, H. Ohashi, M. Haruta, Gold clusters supported on alkaline treated TS-1 for highly efficient propene epoxidation with O_2 and H_2, Appl. Catal. B 95 (2010) 430–438.

14. X. Feng, Y. B. Liu, Y. C. Li, C.H. Yang, Z.H Zhang, X.Z. Duan, X.G Zhou, Au/TS-1 catalyst for propene epoxidation with H_2/O_2: a novel strategy to enhance stability by tuning charging sequence, AIChE J. 62 (2016) 3963-3972.

15. A. Ruiz, B.V.D. Linden, M. Makkee, G. Mul, Acrylate and propoxy-groups: contributors to deactivation of Au/TiO_2 in the epoxidation of propene, J. Catal. 266 (2009) 286-290.

16. H. Wang, T.J. Pinnavaia, MFI zeolite with small and uniform intracrystal mesopores, Angew. Chem. Int. Edit. 45 (2006) 7603-7606.

17. X. Feng, X. Duan, J. Yang, G. Qian, X. Zhou, D. Chen, W. Yuan, Au/uncalcined TS-1 catalysts for direct propene epoxidation with H_2 and O_2: effects of Si/Ti molar ratio and Au loading, Chem. Eng. J. 278 (2015) 234-239.

18. X. Feng, D. Chen, X. Zhou, Thermal stability of TPA template and size-dependent selectivity of uncalcined TS-1 supported Au catalyst for propene epoxidation with H_2 and O_2, Rsc Adv. 50 (2016) 44050-44056.

19. X. Feng, N. Sheng, Y. Liu, X. Chen, D. Chen, C. Yang, X. Zhou, Simultaneously enhanced stability and selectivity for propene epoxidation with H_2 and O_2 on Au catalysts supported on nano-crystalline mesoporous TS-1, ACS Catal. 7 (2017) 2668-2675.

20. T. Iwasaki, M. Isaka, H. Nakamura, M. Yasuda, S. Watano, Synthesis of titanosilicate TS-1 crystals via mechanochemical route using low cost materials, Micropor. Mesopor. Mat. 150 (2012) 1-6.

21. Y. Zuo, X. Wang, X. Guo, Synthesis of titanium silicalite-1 with small crystal size by using mother liquid of titanium silicalite-1 as seed, Ind. Eng. Chem. Res. 50 (2011) 8485–8491.

22. Z.N. Song, X. Feng, N. Sheng, D. Lin, Propene epoxidation with H_2 and O_2 on Au/TS-1 catalyst: cost-effective synthesis of small-sized mesoporous TS-1 and its unique performance, Catal. Today. DOI.org/10.1016/j.cattod.2018.04.068.

23. Y. Zhao, H. Li, H. Li, NiCo@ SiO_2 core-shell catalyst with high activity and long lifetime for CO_2 conversion through DRM reaction, Nano Energy 45 (2018) 101–108.

24. C.S. Cundy, J.O. Forrest, R.J. Plaisted, Some observations on the preparation and properties of colloidal silicalites Part I: synthesis of colloidal silicalite-1 and titanosilicalite-1 (TS-1), Micropor. Mesopor. Mat. 66 (2003) 143-156.

25. G. Zhan, M. Du, D. Sun, J. Huang, X. Yang, Vapor-phase propylene epoxidation with H_2/O_2 over bioreduction Au/TS-1 catalysts: synthesis, characterization, and optimization, Ind. Eng. Chem. Res. 50 (2011) 9019-9026.

26. X. Feng, X. Duan, H Cheng, G. Qian, D. Chen, W. Yuan, X. Zhou, Au/TS-1 catalyst prepared by deposition–precipitation method for propene epoxidation with H_2/O_2: insights into the effects of slurry aging time and Si/Ti molar ratio, J. Catal. 325 (2015) 128-135.

27. R.B. Khomane, B.D. Kulkarni, A. Paraskar, S.R. Sainkar, Synthesis, characterization and catalytic performance of titanium silicalite-1 prepared in micellar media, Mater. Chem. Phys. 76 (2002) 99-103.

28. S. Mintova, M. Hölzl, V. Valtchev, B. Mihailova, Y. Bouizi, Closely packed zeolite nanocrystals obtained via transformation of porous amorphous silica, Chem. Mater. 16 (2004) 5452-5459.

29. S. Bordiga, F. Bonino, A. Damin, C. Lamberti, Reactivity of Ti(IV) species hosted in TS-1 towards H_2O_2-H_2O solutions investigated by ab initio cluster and periodic approaches combined with experimental XANES and EXAFS data: a review and new highlights, Phys. Chem. Chem. Phys. 9 (2007) 4854-4878.

30. J. Su, G. Xiong, J. Zhou, W. Liu, D. Zhou, G. Wang, X. Wang, H. Guo, Amorphous Ti species in titanium silicalite-1: structural features, chemical properties, and inactivation with sulfosalt, J. Catal. 288 (2012) 1-7.

31. G.N. Vayssilov, Structural and physicochemical features of titanium silicalites, Catal. Rev. 39 (1997) 209-251.

32. L. Xu, Y. Ren, H. Wu, Y. Liu, Z. Wang, Y. Zhang, J. Xu, H. Peng, P. Wu, Core/shell-structured TS-1@mesoporous silica-supported Au nanoparticles for selective epoxidation of propylene with H_2 and O_2, J. Mater. Chem. 21 (2011) 10852-10858.

33. Z. Wang, L. Xu, J.G. Jiang, Y. Liu, M. He, P. Wu, One-pot synthesis of catalytically active and mechanically robust mesoporous TS-1 microspheres with the aid of triblock copolymer, Micropor. Mesopor. Mat. 156 (2012) 106-114.

34. C. Shen, Y. Wang, J. Xu, G. Luo, Synthesis of TS-1 on porous glass beads for catalytic oxidative desulfurization, Chem. Eng. J. 259 (2015) 552-561.

35. B. Xie, H. Zhang, C. Yang, S. Liu, L. Ren, Seed-directed synthesis of zeolites with enhanced performance in the absence of organic templates, Chem. Commun. 47 (2011) 3945-3947.

36. K. Itabashi, Y. Kamimura, K. Iyoki, A. Shimojima, T. Okubo, A working hypothesis for broadening framework types of zeolites in seed-assisted synthesis without organic structure-directing agent, J. Am. Chem. Soc. 2012. 134(28): p. 11542-11549.

37. Z.A. Lethbridge, J.J. Williams, R.I. Walton, K.E. Evans, C.W. Smith, Methods for the synthesis of large crystals of silicate zeolites, Micropor. Mesopor. Mat. 79 (2005) 339-352.

38. S. Mintova, J.P. Gilson, V. Valtchev, Advances in nanosized zeolites, Nanoscale 5 (2013) 6693-6703.

39. X. Li, Y. Peng, Z. Wang, Y. Yan, Synthesis of highly b-oriented zeolite MFI films by suppressing twin crystal growth during the secondary growth, CrystEngComm 13 (2011) 3657-3660.

40. L. Ding, Y. Zheng, Effect of template concentration and gel dilution on crystallization and particle size of zeolite beta in the absence of alkali cations, Micropor. Mesopor. Mat. 103 (2007) 94-101.

41. X. Feng, X. Duan, G. Qian, X. Zhou, D. Chen, W. Yuan, Insights into size-dependent activity and active sites of Au nanoparticles supported on TS-1 for propene epoxidation with H_2 and O_2, J. Catal. 317 (2014) 99-104.

42. C. Qi, J. Huang, S. Bao, H. Su, T. Akita, Switching of reactions between hydrogenation and epoxidation of propene over Au/Ti-based oxides in the presence of H_2 and O_2, J. Catal. 281 (2011) 12-20.

43. C. Perego, A. Carati, P. Ingallina, M.A. Mantegazza, G. Bellussi, Production of titanium containing molecular sieves and their application in catalysis, Appl. Catal. A-Gen. 221 (2001) 63-72.

44. W. Song, G. Xiong, H. Long, F. Jin, L. Liu, Effect of treatment with different bases on the catalytic properties of TS-1/SiO_2 extrudates in propylene epoxidation, Micropor. Mesopor. Mat. 212 (2015) 48-55.

45. T.A. Nijhuis, T. Visser, B.M. Weckhuysen, The role of gold in gold– titania epoxidation catalysts, Angew. Chem. Int. Edit. 44 (2010) 1115-1118.

46. G. Li, X. Wang, X. Guo, S. Liu, Q. Zhao, Titanium species in titanium silicalite TS-1 prepared by hydrothermal method, Mater. Chem. Phys. 71 (2001) 195-201.

47. J.K. Edwards, B. Solsona, N.N. Edwin, A.F. Carley, Switching off hydrogen peroxide hydrogenation in the direct synthesis process, Science. 323 (2009) 1037-1041.

48. X. Feng, J. Yang, X.Z. Duan, Y. Cao, B. Chen, Enhanced catalytic performance for propene epoxidation with H_2 and O_2 over bimetallic Au-Ag/Uncalcined TS-1 catalysts, ACS Catal. 8 (2018) 7799–7808.

49. J.J. Bravo-Suarez, K.K. Bando, J. Lu, M. Haruta, T. Fujitani, T. Oyama, Transient technique for identification of true reaction intermediates: hydroperoxide species in propylene epoxidation on gold/titanosilicate catalysts by X-ray absorption fine structure spectroscopy, J. Phys. Chem. C 112 (2008) 1115-1123.

50. Y.S. Yong, E.M. Kennedy, N.W. Cant, Oxide catalysed reactions of ethylene oxide under conditions relevant to ethylene epoxidation over supported silver, Appl. Catal. 76 (1991) 31-48.

51. L.D. Rollmann, Systematics of shape selectivity in common zeolites, J. Catal. 47 (1977) 113-121.

52. Z. Li, Y. Wang, J. Zhang, D. Wang, W. Ma, Better performance for gas-phase epoxidation of propylene using H_2 and O_2 at lower temperature over Au/TS-1 catalyst, Catal. Commun. 90 (2017) 87–90.

53. X. Wang, X. Zhang, Y. Wang, H. Liu, J. Wang, J. Qiu, Preparation and performance of TS-1/SiO_2 egg-shell catalysts, Chem. Eng. J. 175 (2011) 408–416.

54. Z. Wu, S. Goel, M. Choi, E. Iglesia, Hydrothermal synthesis of LTA-encapsulated metal clusters and consequences for catalyst stability, reactivity, and selectivity, J. Catal. 311 (2014) 458-468.

55. S. Du, X. Chen, Q. Sun, N. Wang, M. Jia, A non-chemically selective top-down approach towards the preparation of hierarchical TS-1 zeolites with improved oxidative desulfurization catalytic performance, Chem. Commun. 52 (2016) 3580-3583.

56. M. Du, G. Zhan, X. Yang, H. Wang, W. Lin, Ionic liquid-enhanced immobilization of biosynthesized Au nanoparticles on TS-1 toward efficient catalysts for propylene epoxidation, J. Catal. 283 (2011) 192-201.

57. S. Kanungo, D.M.P. Ferrandez, F. Angelo, J.C. Schouten, T.A. Nijhuis, Kinetic study of propene oxide and water formation in hydro-epoxidation of propene on Au/Ti–SiO_2 catalyst, J. Catal. 338 (2016) 284-294.

Table captions:

Table 1 Catalytic properties of stable Au/Ti-containing catalysts for propene epoxidation with H_2 and O_2

Table 1 Catalytic properties of stable Au/Ti-containing catalysts for propene epoxidation with H_2 and O_2

Samples	Au loading (wt%)	PO selectivity (%)	PO formation rate ($g_{PO}h^{-1}kg_{Cat}^{-1}$)	Stability [a] (h)	Reaction temperature (K)	Reference
Au/TS-1/S-1	0.10	87.2	140	100	473	This work
Au/TS-1-1L	1.0	65	75	48	473	[56]
Au/MTS-1	0.13	95.2	142	40	473	[19]
Au/TS-1-B	0.12	83	125	30	473	[17]
Au/TS-1-SG	0.10	85.0	119	21	473	[13]
Au/Ti-SiO_2	0.1	90.0	100	5	473	[57]

[a] It should be noted that the stable time-on-tream of catalysts could be longer although it is not reported.

Figure captions:

Fig. 1. XRD spectra (a) and N_2 adsorption-desorption isotherms (b) of TS-1/S-1 and conventional TS-1 samples. The inset in Fig.1b shows the pore size distributions.

Fig. 2. FT-IR spectra (a) and UV-vis spectra (b) of TS-1/S-1 and conventional TS-1 samples.

Fig. 3. TEM images of S-1 seed (a) and TS-1/S-1 (b).

Fig. 4. Schematic diagram of crystallization process.

Fig. 5. HRTEM image of TS-1/S-1.

Fig. 6. XRD patterns of TS-1/S-1 samples with different TPAOH/SiO_2 molar ratios.

Fig. 7. FT-IR spectra (a) and UV-vis spectra (b) of TS-1/S-1 samples with different TPAOH/SiO_2 molar ratios.

Fig. 8. TEM images of TS-1/S-1 samples with different TPAOH/SiO_2 molar ratios of 0 (a), 0.005 (b), 0.01 (c) and 0.02 (d).

Fig. 9. HRTEM images of Au/TS-1 (a), Au/TS-1-TPA-0.005/S-1 (b), Au/TS-1-TPA-0.01/S-1 (c) and Au/TS-1-TPA-0.02/S-1 (d) catalysts. The insets show the Au size distributions of the catalysts, and the scale bars represent 2 nm.

Fig. 10. PO formation rate (a) and detailed products selectivities and H_2 efficiencies (b) of Au/TS-1 and Au/TS-1/S-1 catalysts at different time-on-stream.

Fig. 11. TGA (a) and DTG (b) curves of Au/TS-1/S-1 and Au/TS-1 catalysts at 200 ^oC for 20 h.

Fig. 12. FT-IR spectra of Au/TS-1/S-1 and Au/TS-1 catalysts at 200 ^oC for 20 h.

Fig. 13. ^{29}Si MAS NMR spectra of TS-1 (a) and TS-1/S-1 (b) supports.

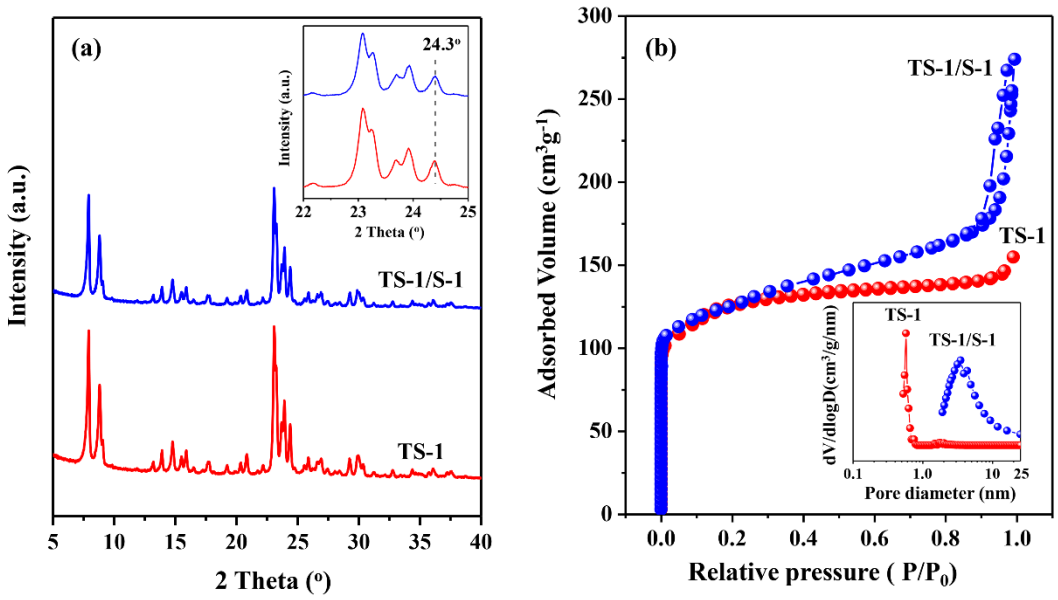

Fig. 1. XRD spectra (a) and N_2 adsorption-desorption isotherms (b) of TS-1/S-1 and conventional TS-1 samples. The inset in Fig.1b shows the pore size distributions.

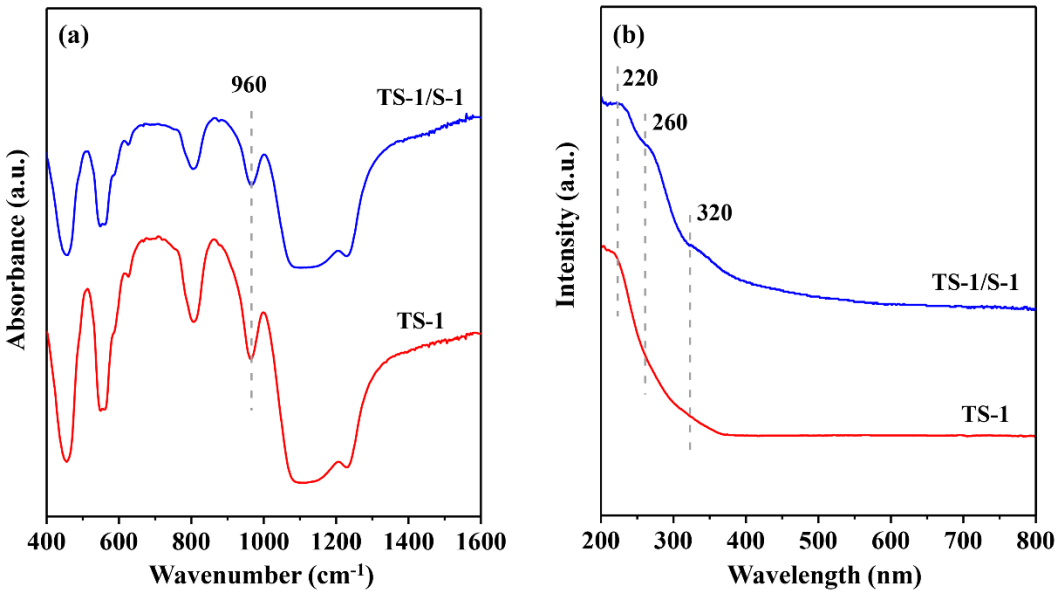

Fig. 2. FT-IR spectra (a) and UV-vis spectra (b) of TS-1/S-1 and conventional TS-1 samples.

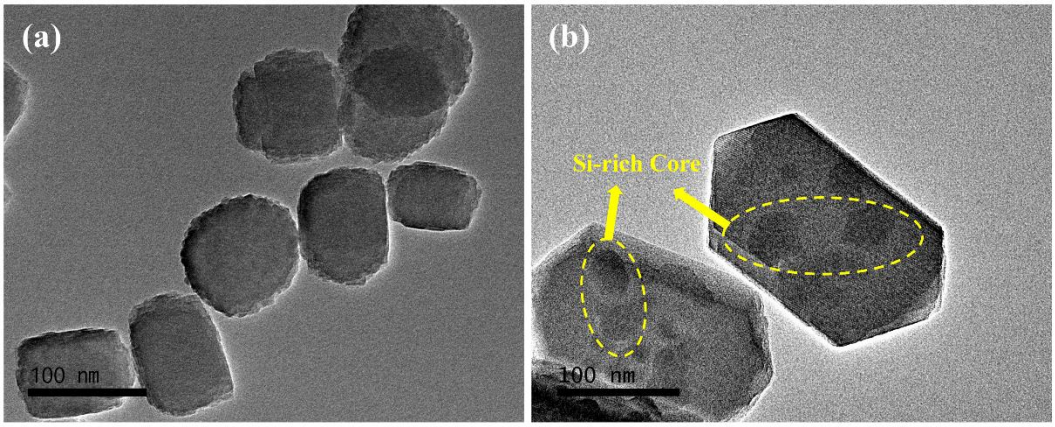

Fig. 3. TEM images of S-1 seed (a) and TS-1/S-1 (b).

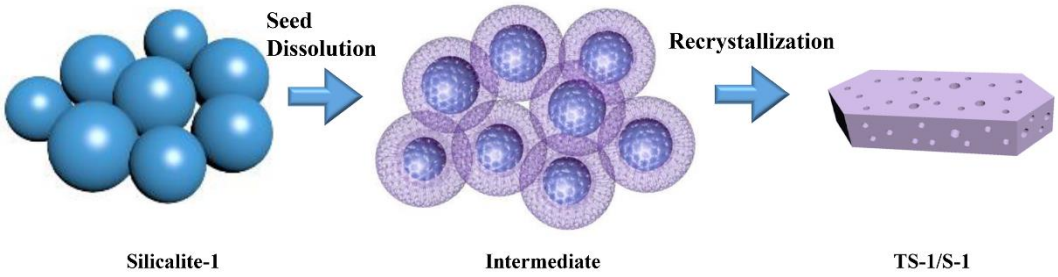

Fig. 4. Schematic diagram of crystallization process.

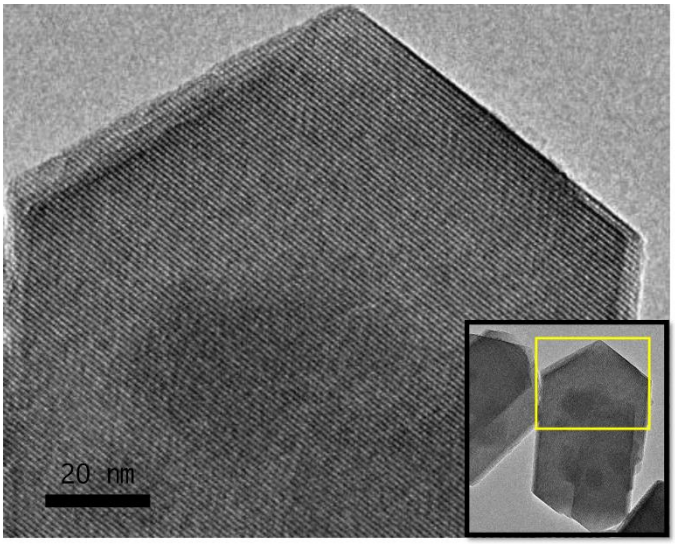

Fig. 5. HRTEM image of TS-1/S-1.

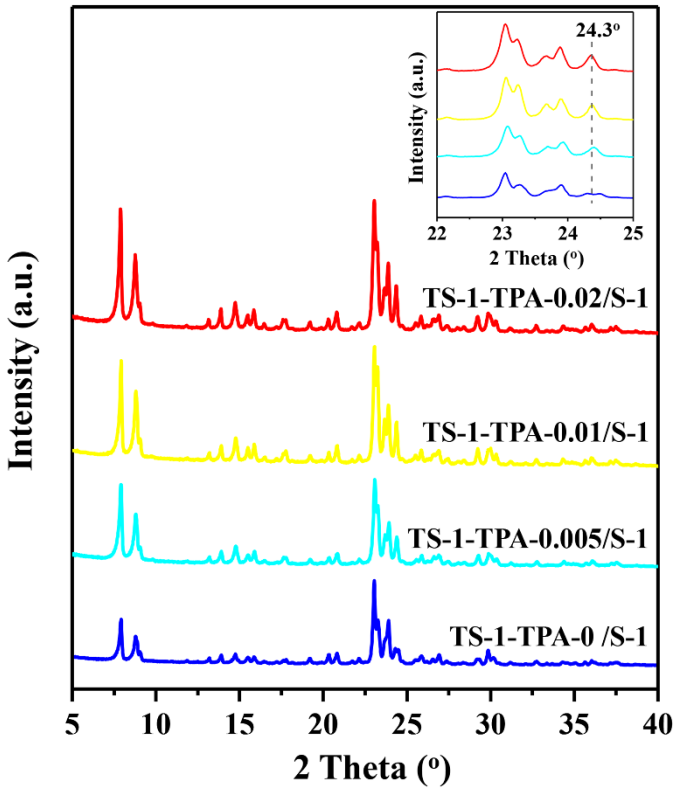

Fig. 6. XRD patterns of TS-1/S-1 samples with different TPAOH/SiO_2 molar ratios.

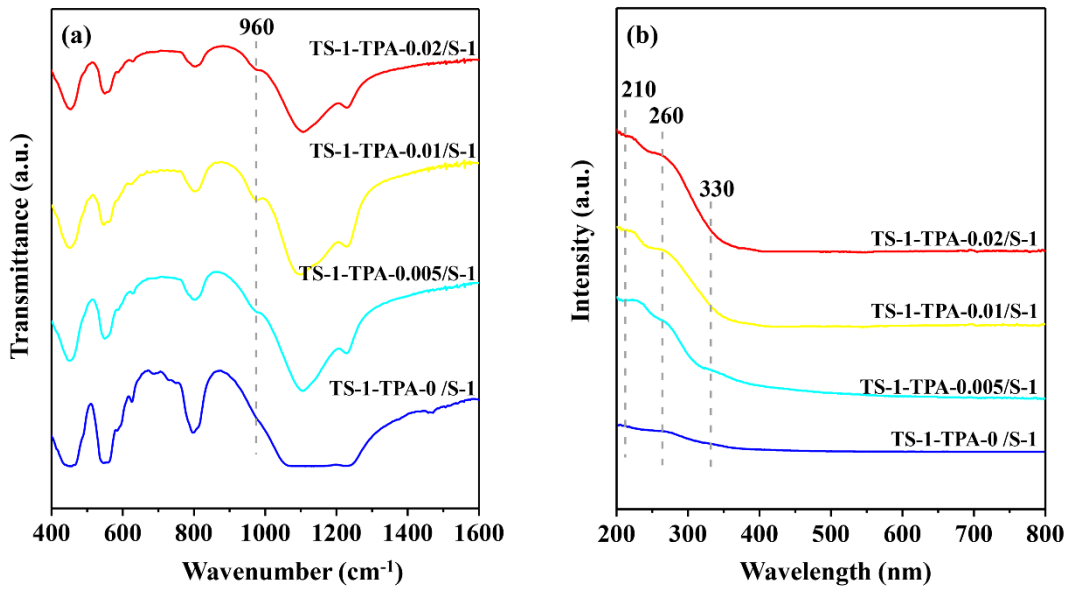

Fig. 7. FT-IR spectra (a) and UV-vis spectra (b) of TS-1/S-1 samples with different TPAOH/SiO_2 molar ratios.

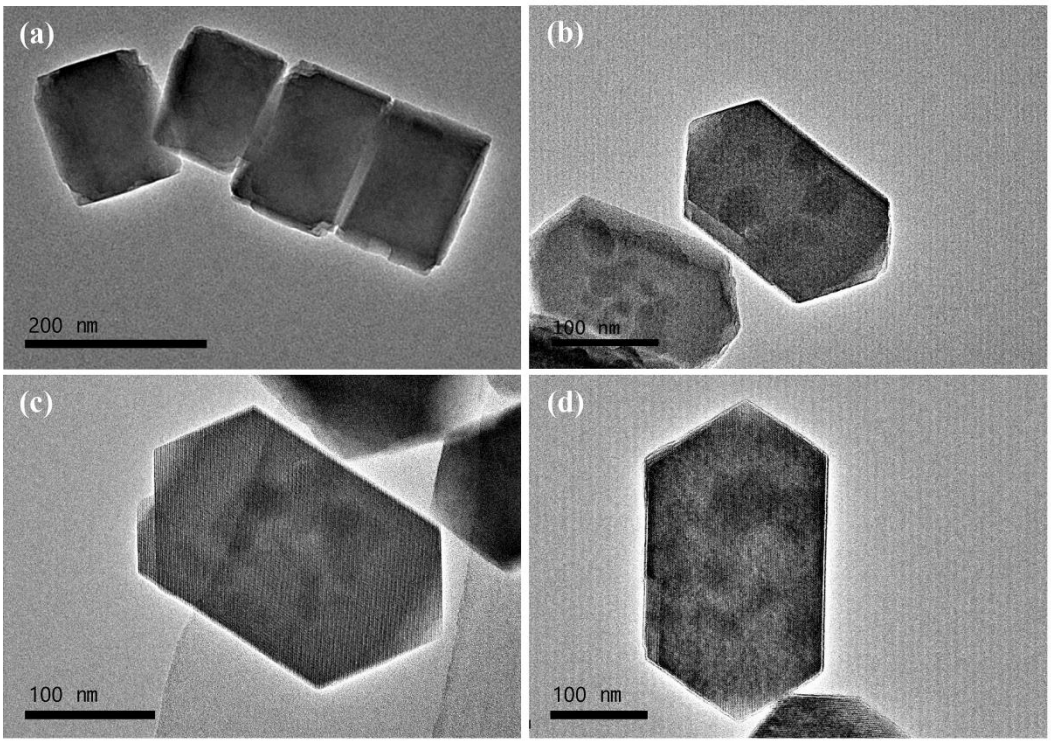

Fig. 8. TEM images of TS-1/S-1 samples with different TPAOH/SiO_2 molar ratios of 0 (a), 0.005 (b), 0.01 (c) and 0.02 (d).

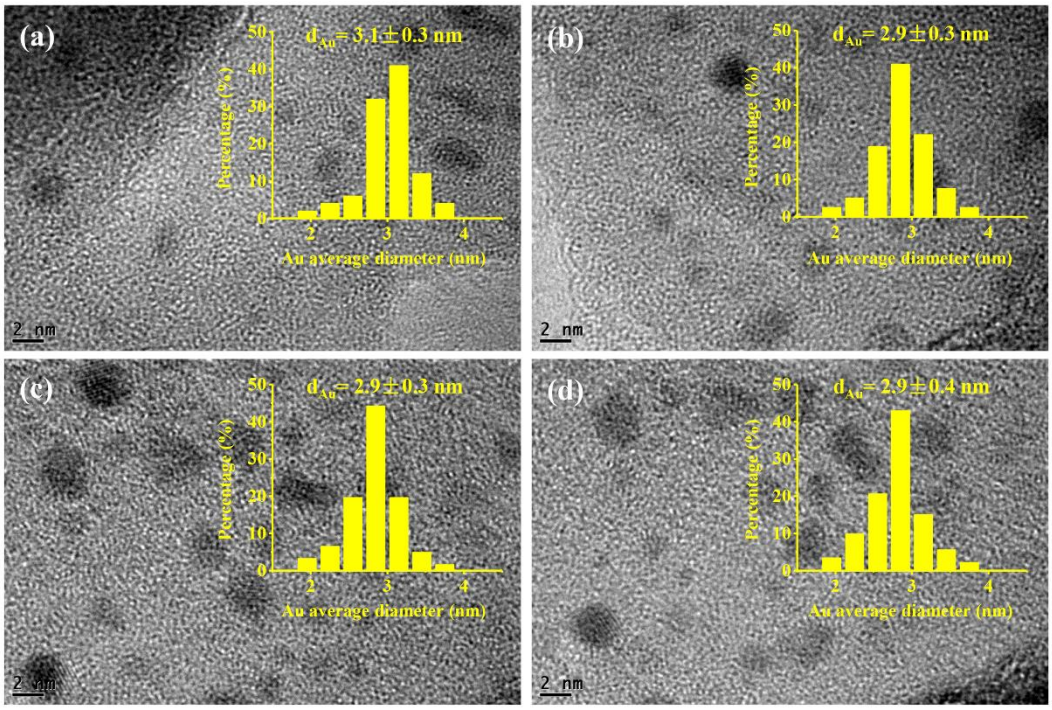

Fig. 9. HRTEM images of Au/TS-1 (a), Au/TS-1-TPA-0.005/S-1 (b), Au/TS-1-TPA-0.01/S-1 (c) and Au/TS-1-TPA-0.02/S-1 (d) catalysts. The insets show the Au size distributions of the catalysts, and the scale bars represent 2 nm.

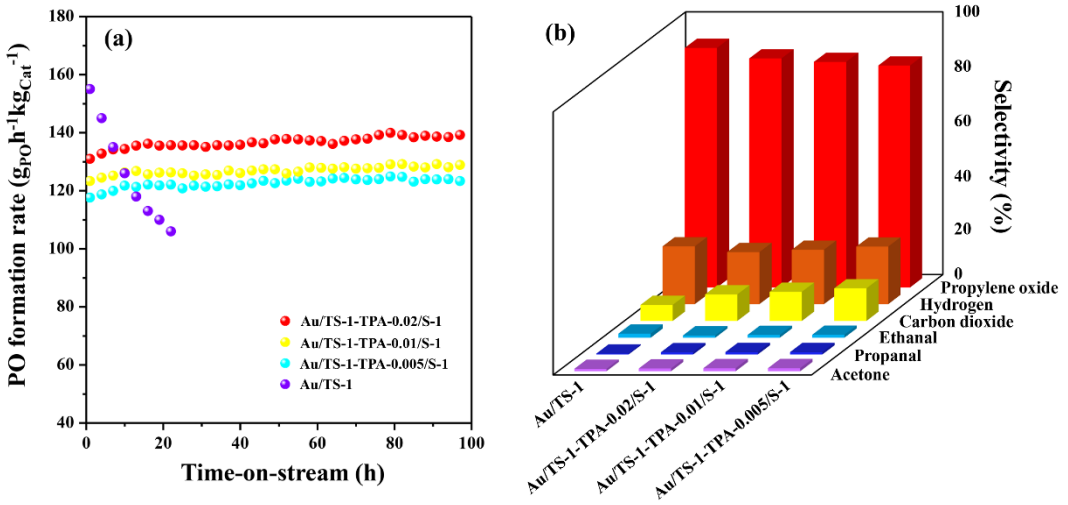

Fig. 10. PO formation rate (a) and detailed products selectivities and H_2 efficiencies (b) of Au/TS-1 and Au/TS-1/S-1 catalysts at different time-on-stream.

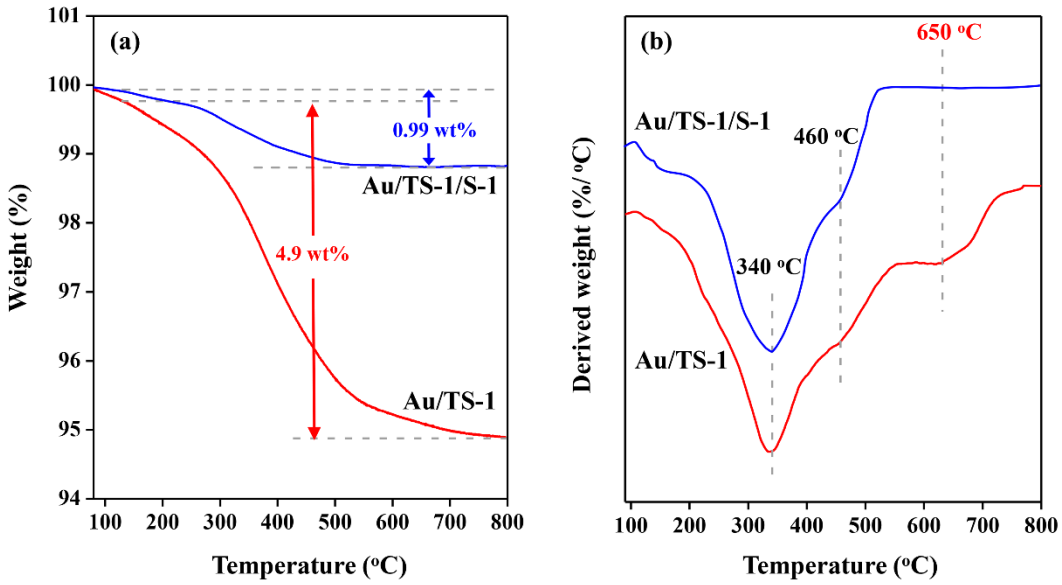

Fig. 11. TGA (a) and DTG (b) curves of Au/TS-1/S-1 and Au/TS-1 catalysts at 200 °C for 20 h.

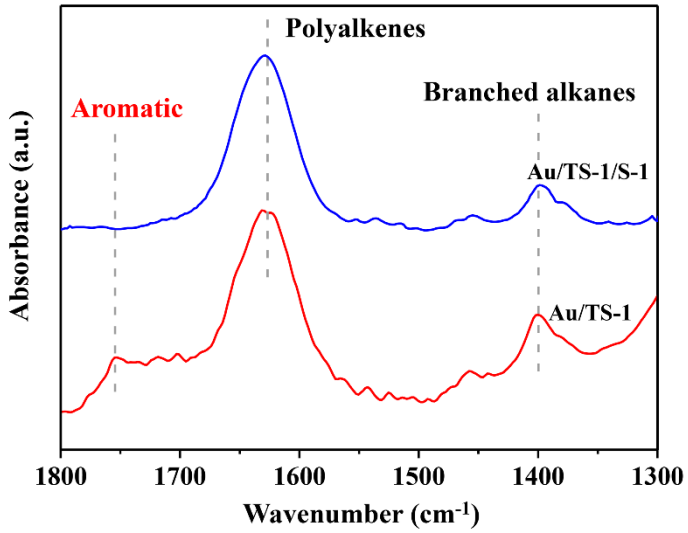

Fig. 12. FT-IR spectra of Au/TS-1/S-1 and Au/TS-1 catalysts at 200 °C for 20 h.

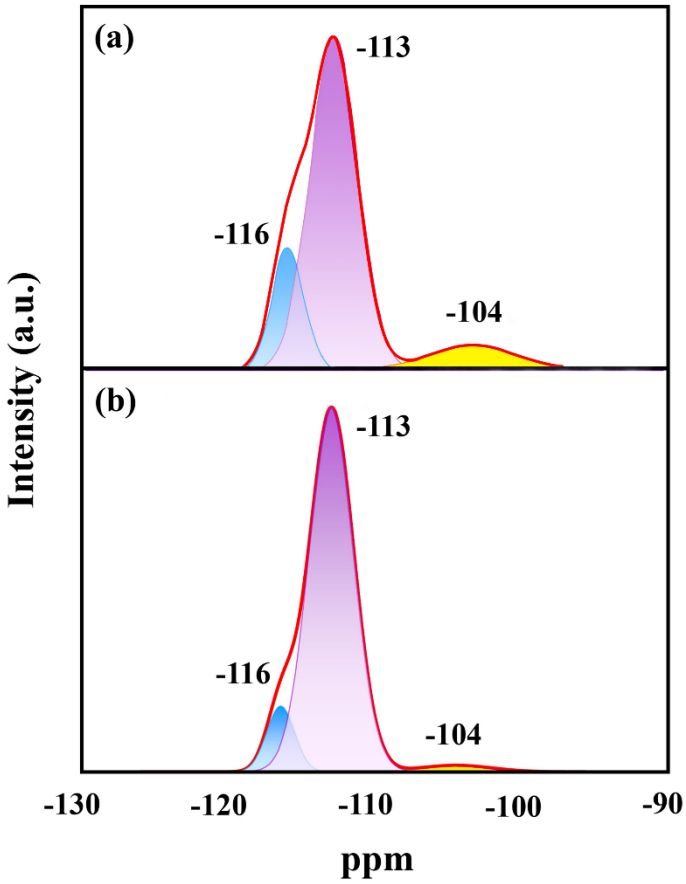

Fig. 13. ^{29}Si MAS NMR spectra of TS-1 (a) and TS-1/S-1 (b) supports. The total integral curve is the red line.